

# Non-trivial class of anisotropic compact stellar model in Rastall gravity

G. Nashed<sup>1</sup>, and K. Bamba<sup>2</sup>

<sup>1</sup>Centre for Theoretical Physics, The British University in Egypt,  
P.O. Box 43, El Sherouk City, Cairo 11837, Egypt

<sup>2</sup> Faculty of Symbiotic Systems Science, Fukushima University,  
Fukushima 960-1296, Japan

The details of the present presentation is presented in [2208.13814](#)

# Introduction

The topic of stellar structure has been developed over many years either in Newtonian gravity or later in General Relativity (GR). Motivated by the claim that pressure at core of the compact star model could have anisotropic structure many models have been developed imposing the anisotropic pressure concept (assuming radial and tangential pressures are different) to derive realistic stellar models within the GR context and in modified gravity as well. The GR theory has been proven to be a successful theory of gravity on solar system scales by many observational tests and also on black hole scales using black hole shadows observations by Event Horizon Telescope.

# Introduction

On the cosmological scales, the GR does not provide answers for explaining the late accelerated expansion. Even in presence of a cosmological constant  $\Lambda$ , the discrepancy of the current Hubble parameter  $H_0$  value, between early universe observations by Planck satellite and late universe measurements by distance ladder or strong lensing, may point out the need to modify the GR theory. Many efforts have been done to generalize GR theory by using general function in Einstein-Hilbert action instead of the Ricci invariant, e.g.  $f(R)$ ,  $f(G)$ ,  $f(T)$  and mimetic gravity.

# Introduction

In fact, these modified theories kept the fundamental assumption that the covariant divergence of the energy-momentum vanishes, i.e.  $\mathcal{T}^\alpha{}_{\beta;\alpha} = 0$  where the semicolon denotes the Levi-Civita covariant derivative. On the contrary, Rastall attempted to modify GR by dropping this assumption replacing it by setting  $\mathcal{T}^\alpha{}_{\beta;\alpha} = a_\beta$  where  $a_\beta$  vanishes in flat spacetime (vacuum) and recovers GR, otherwise it does not<sup>1</sup>. Rastall showed that  $a_\beta \propto \partial_\beta \mathcal{R}$  is a reasonable choice which reflects the non-minimal coupling between matter and geometry. Interestingly, some cosmological models have been constructed using  $\mathcal{R}T^2$

---

<sup>1</sup>Rastall, Phys. Rev. D **6**, 3357 (1972)

<sup>2</sup>C.E.M. Batista, M.H. Daouda, J.C. Fabris, O.F. Piattella, D.C. Rodrigues, Phys. Rev. D **85**, 084008 (2012)

# Introduction

as well as black hole solutions<sup>3</sup>.

Recently, Visser claimed that RT is completely equivalent to GR<sup>4</sup>. On the contrary, Darabi et al. investigated Visser's claim but they concluded that Visser misinterpreted the matter-geometry coupling term which led him to wrong conclusion<sup>5</sup>. In addition, they showed that by applying Visser's approach to  $f(R)$  theory one may conclude that it is equivalent to GR as well which is not true.

---

<sup>3</sup>K. Bamba, A. Jawad, S. Rafique, H. Moradpour, The EPJC **78**(12), 1 (2018)

<sup>4</sup>M. Visser, Phys. Lett. B **782**, 83 (2018).

<sup>5</sup>F. Darabi, H. Moradpour, I. Licata, Y. Heydarzade, C. Corda, Eur. Phys. J. C **78**, 25 (2018)

# Introduction

Different studies have proven that RT is not equivalent to GR<sup>6</sup>. Visser's conclusion is correct when Ricci scalar vanishes for black holes in general, otherwise the claim is incorrect and both theories are not equivalent. One of the good examples which may reveal the contribution of the matter-geometry coupling in RT in contrast to GR is the stellar models when the presence of matter plays a crucial role. It is the aim of the present study to derive an anisotropic static spherically symmetric interior solution using RT and confront it with pulsars observations.

---

<sup>6</sup>S. Hansraj, A. Banerjee, P. Channuie, *Annals Phys.* **400**, 320 (2019) 

# Rastall gravitational theory

In Riemann geometry, by making use of the contracted Bianchi Identity on one hand and the minimal coupling procedure on the other hand,

$$\mathcal{G}_{\alpha\beta;\alpha} = (\mathcal{R}_{\alpha\beta} - \frac{1}{2}g_{\alpha\beta}\mathcal{R});_{\alpha} \equiv 0, \quad \mathcal{T}_{\alpha\beta;\alpha} = 0, \quad (1)$$

this led Einstein to formulate the consistent field equations of GR

$$\mathcal{G}_{\alpha\beta} = \chi\mathcal{T}_{\alpha\beta}, \quad (2)$$

where  $\chi = 8\pi G_N/c^4$  where  $G_N$  is the Newtonian gravitational constant and  $c$  is the speed of light,  $\mathcal{G}_{\alpha\beta}$  denotes Einstein tensor,  $\mathcal{R}_{\alpha\beta}$  denotes Ricci tensor and  $\mathcal{R} = g^{\alpha\beta}\mathcal{R}_{\alpha\beta}$  denotes Ricci invariant.

# Rastall gravitational theory

Rastall, however, dropped the minimal coupling procedure assuming non-divergence-free energy-momentum in curved spacetime

$$\mathcal{T}^\alpha{}_{\beta;\alpha} \neq 0, \quad \mathcal{T}^\alpha{}_{\beta;\alpha} = \mathbf{a}_\beta = \tilde{\epsilon} \partial_\beta \mathcal{R}, \quad (3)$$

where the constant of proportionality  $\tilde{\epsilon}$  measures how much the conservation law is locally violated. According to this assumption Rastall obtained a consistent set of field equations

$$\mathcal{G}_{\alpha\beta} = \mathcal{R}_{\alpha\beta} - \frac{1}{2} g_{\alpha\beta} \mathcal{R} = \chi (\mathcal{T}_{\alpha\beta} - \tilde{\epsilon} g_{\alpha\beta} \mathcal{R}). \quad (4)$$



# Rastall gravitational theory

Alternatively, Eq. (4) can be rewritten as

$$\mathcal{R}_{\alpha\beta} - \left(\frac{1}{2} - \chi\tilde{\epsilon}\right)g_{\alpha\beta}\mathcal{R} = \chi\mathcal{T}_{\alpha\beta}. \quad (5)$$

Contracting the above equation gives

$$(1 - 4\chi\tilde{\epsilon})\mathcal{R} = -\chi\mathcal{T}, \quad (6)$$

where  $\mathcal{T} = g^{\alpha\beta}\mathcal{T}_{\alpha\beta}$  is the trace of the energy-momentum tensor. Thus the field equations of RT read

$$\mathcal{G}_{\alpha\beta} = \chi\tilde{\mathcal{T}}_{\alpha\beta}. \quad (7)$$

where

$$\tilde{\mathcal{T}}_{\alpha\beta} = \mathcal{T}_{\alpha\beta} + \frac{\chi\tilde{\epsilon}}{1 - 4\chi\tilde{\epsilon}}g_{\alpha\beta}\mathcal{T}, \quad 1 - 4\chi\tilde{\epsilon} \neq 0. \quad (8)$$

# Rastall gravitational theory

It proves convenient to use a dimensionless Rastall's parameter  $\epsilon = \tilde{\epsilon}\chi$ , c.f.<sup>7</sup>. Then, Eq. (5) becomes

$$\mathcal{R}_{\alpha\beta} - \left(\frac{1}{2} - \epsilon\right)g_{\alpha\beta}\mathcal{R} = \chi\mathcal{T}_{\alpha\beta}, \quad (9)$$

and the tensor  $\tilde{\mathcal{T}}_{\alpha\beta}$  in Eq. (7) reads

$$\tilde{\mathcal{T}}_{\alpha\beta} = \mathcal{T}_{\alpha\beta} + \frac{\epsilon}{1-4\epsilon}g_{\alpha\beta}\mathcal{T}, \quad \epsilon \neq \frac{1}{4}. \quad (10)$$

For  $\epsilon = 0$  case, the conservation law is restored and the GR version of gravity is recovered. In this sense, RT generalizes Einstein's one by assuming a local violation of conservation law in curved spacetime due to non-minimal coupling between matter and geometry.

<sup>7</sup>A.M. Oliveira, H.E.S. Velten, J.C. Fabris, L. Casarini, Phys. Rev. D **92**(4), 044020 (2015)

## spherically symmetric interior solution

Otherwise, flat spacetime, both theories are equivalent. Therefore, one of the important applications, which differentiate both theories, is stellar structure models when presence of the matter sector plays a crucial role in interior solutions. Providing that the static spherically symmetrical spacetime is given by the following metric<sup>8</sup>

$$ds^2 = -F(r)dt^2 + G(r)dr^2 + r^2(d\theta^2 + \sin^2\theta d\phi^2), \quad (11)$$

where  $F(r)$  and  $G(r)$  are unknown functions. The Ricci scalar of the above line-element takes the form:

$$\mathcal{R}(r) = \frac{-2F''GFr^2 + F'^2Gr^2 + rFF'(rG' - 4G) + 4F^2[rG' + G(G - 1)]}{2F^2G^2r^2}. \quad (12)$$

---

<sup>8</sup>We take the geometric units which set  $\chi = c = 1$ .

## spherically symmetric interior solution

We assume the energy-momentum tensor for a anisotropic fluid with spherical symmetry, i.e.

$$\mathcal{T}^{\alpha}_{\beta} = (p_t + \rho)u^{\alpha}u_{\beta} + p_t\delta^{\alpha}_{\beta} + (p_r - p_t)\zeta^{\alpha}\zeta_{\beta}, \quad (13)$$

where  $\rho = \rho(r)$  is the fluid energy density,  $p_r = p_r(r)$  its radial pressure (in the direction the time-like four-velocity  $u_{\alpha}$ ),  $p_t = p_t(r)$  its tangential pressure (perpendicular to  $u_{\alpha}$ ) and  $\zeta^{\alpha}$  is the unit space-like vector in the radial direction. Then, the energy-momentum tensor takes the diagonal form  $\mathcal{T}^{\alpha}_{\beta} = \text{diag}(-\rho, p_r, p_t, p_t)$ .

## spherically symmetric interior solution

Applying Rastall's field equations (7) to the spacetime (11) where the matter sector is as given by (13) we obtain, respectively, the components  $tt$ ,  $rr$  and  $\theta\theta$  ( $= \phi\phi$ ) as follows:

$$\begin{aligned} \rho &= \frac{rG' + G(G-1)}{G^2 r^2} - \frac{\epsilon}{1-4\epsilon}(\rho - p_r - 2p_t), \\ p_r &= \frac{F'r - F(G-1)}{FG r^2} + \frac{\epsilon}{1-4\epsilon}(\rho - p_r - 2p_t), \\ p_t &= \frac{F[2G(F''r + F') - G'F'r] - 2G'F^2 - F'^2 Gr}{4F^2 G^2 r} + \frac{\epsilon}{1-4\epsilon}(\rho - p_r - 2p_t). \end{aligned} \quad (14)$$

Additionally, we define the anisotropy of the system (14) using the parameter

$$\Delta(r) = p_t - p_r = \frac{2F''GFr^2 - F'^2 Gr^2 - rFF'(rG' + 2G) - 2F^2[rG' - 2G(G-1)]}{4F^2 G^2 r^2}. \quad (15)$$

## spherically symmetric interior solution

First, we assume the metric potential  $G$  to have the form

$$G(r) = \frac{1}{\left(1 - \frac{a_2^2 r^2}{R^2}\right)^4}, \quad (16)$$

with  $a_2$  is a dimensionless constant to be determined by boundary condition and  $R$  is the radius at the star boundary. We note that the above ansatz is regular everywhere inside the star, i.e.

$0 \leq r \leq R$ , where  $|a_2| < 1$ . Substituting (16) in the anisotropy parameter (15), we get

$$\Delta(r) = \frac{a_2^4 r^2 (6R^4 - 8R^2 a_2^2 r^2 + 3a_2^4 r^4)}{R^8} + \frac{(R^2 - a_2^2 r^2)^3 [r(2FF'' - F'^2)(R^2 - a_2^2 r^2) - 2FF'(R^2 + 3a_2^2 r^2)]}{4rF^2 R^8}. \quad (17)$$

## spherically symmetric interior solution


Now, we impose the second condition by assuming that the component  $g_{tt}$  has no contribution on the anisotropy parameter, i.e.

$$\Delta(r) = \frac{a_2^4 r^2 (6R^4 - 8R^2 a_2^2 r^2 + 3a_2^4 r^4)}{R^8}. \quad (18)$$

This choice clearly gives no anisotropy at the center,  $r = 0$ , which is physically a reasonable feature. Using Eqs. (17) and (18) and by solving for the metric potential  $F$ , we obtain:

$$F(r) = \frac{[a_0 R^2 + 2a_1 a_2^2 (R^2 - a_2^2 r^2)]^2}{8a_2^4 (R^2 - a_2^2 r^2)^2}, \quad (19)$$

where the constants of integration  $a_0$  and  $a_1$  are dimensionless to be fixed by matching conditions. Up to this step the obtained results are the same as given by<sup>9</sup>.

<sup>9</sup>S. Das, F. Rahaman, L. Baskey, EPJC (10), 853 (2019). 

# spherically symmetric interior solution

Substituting the metric potentials (16) and (19) into the system (14), we get the energy-density, radial and tangential pressures in the form

$$\begin{aligned}
 \rho &= \frac{12a_2^2}{R^8 [2a_1 a_2^2 (a_2^2 r^2 - R^2) - a_0 R^2]} \left\{ \frac{3a_1 a_2^{10}}{2} (2\epsilon - 1) r^8 - \frac{a_2^6}{2} \left[ \frac{a_1 a_2^2}{3} (74\epsilon - 37) + \frac{a_0}{2} (2\epsilon - 3) \right] R^2 r^6 \right. \\
 &\quad \left. + \frac{a_2^4}{3} [a_1 a_2^2 (58\epsilon - 29) + a_0 (5\epsilon - 7)] R^4 r^4 - 2a_2^2 \left[ \frac{7a_1 a_2^2}{2} (2\epsilon - 1) + \frac{a_0}{4} (4\epsilon - 5) \right] R^6 r^2 + [(4a_1 a_2^2 + a_0)\epsilon - (2a_1 a_2^2 + a_0)] R^8 \right\}, \\
 p_r &= \frac{12a_2^2}{R^8 [2a_1 a_2^2 (R^2 - a_2^2 r^2) + a_0 R^2]} \left\{ \frac{a_1 a_2^{10}}{6} (18\epsilon - 1) r^8 - \frac{a_2^6}{2} \left[ \frac{a_1 a_2^2}{3} (74\epsilon - 5) + \frac{a_0}{2} (2\epsilon + 1) \right] R^2 r^6 \right. \\
 &\quad \left. + \frac{a_2^4}{3} [a_1 a_2^2 (58\epsilon - 5) + a_0 (5\epsilon + 2)] R^4 r^4 - 2a_2^2 \left[ \frac{a_1 a_2^2}{6} (42\epsilon - 5) + \frac{a_0}{4} (4\epsilon + 1) \right] R^6 r^2 + \left[ (4a_1 a_2^2 + a_0)\epsilon - \frac{2}{3} a_1 a_2^2 \right] R^8 \right\}, \\
 p_t &= \frac{12a_2^2}{R^8 [2a_1 a_2^2 (R^2 - a_2^2 r^2) + a_0 R^2]} \left\{ \frac{a_1 a_2^{10}}{3} (9\epsilon - 2) r^8 - \frac{a_2^6}{2} \left[ \frac{2a_1 a_2^2}{3} (74\epsilon - 8) + a_0 \epsilon \right] R^2 r^6 + \frac{a_2^4}{3} [a_1 a_2^2 (58\epsilon - 12) + 5a_0 \epsilon] R^4 r^4 \right. \\
 &\quad \left. - 2a_2^2 \left[ \frac{a_1 a_2^2}{3} (42\epsilon - 4) + a_0 \epsilon \right] R^6 r^2 + \left[ (4a_1 a_2^2 + a_0)\epsilon - \frac{2}{3} a_1 a_2^2 \right] R^8 \right\}.
 \end{aligned} \tag{20}$$



## spherically symmetric interior solution


Equations (20) coincide with the GR version when Rastall parameter  $\epsilon$  vanishes<sup>10</sup>. It is to be mentioned that the anisotropic force,  $F_a = \frac{2\Delta}{r}$ , becomes attractive if  $p_t - p_r < 0$  and repulsive if  $p_t - p_r > 0$ . The mass contained within a radius  $r$  of the sphere is defined as

$$M(r) = 4\pi \int_0^r \rho(\zeta) \zeta^2 d\zeta. \quad (21)$$

Using the energy-density as defined in Eqs. (20) and the above equation (21), we get

$$M(r) = \frac{-3\pi}{a_1^4 a_2^{10} R^8 \aleph} \left\{ \frac{\sqrt{2} a_0 R^9 \epsilon}{2} (a_0 + 2a_1 a_2^2) \tanh^{-1} \left( \frac{\sqrt{2} a_1 a_2^2 r}{R \aleph} \right) + a_2^2 \aleph r \left[ \frac{256 a_1^4 a_2^{10} r^2}{3} (2\epsilon - 1) (2R^2 - a_2^2 r^2) (2R^4 + a_2^4 r^4 - 2a_2^2 R^2 r^2) + a_0 R^2 \epsilon \left( a_0^3 R^6 + \frac{2r^2 a_1 a_2^4}{8} (4a_1^2 a_2^4 - 2a_1 a_2^2 a_0 + a_0^2) R^4 + \frac{4a_1^2 a_2^8 r^4}{5} (a_0 - 4a_1 a_2^2) R^2 + \frac{8a_1^3 a_2^{12} r^6}{7} \right) \right] \right\}, \quad (22)$$

where  $\aleph = \sqrt{(a_0 + 2a_1 a_2^2) a_1}$ .

<sup>10</sup>Z. Roupas, G.G.L. Nashed, Eur. Phys. J. C **80**(10), 905 (2020) 

## spherically symmetric interior solution

It proves convenient to use the compactness parameter of a spherically symmetric source with radius  $r$ ,

$$u(r) = \frac{2M(r)}{r}, \quad (23)$$

to study the stability of compact objects. Similarly we use the gravitational red-shift parameter  $Z$  which is related to the metric potential as

$$1 + Z = \frac{1}{\sqrt{-g_{tt}}}. \quad (24)$$

## Physical conditions for a stellar model

For a stellar model to be physically well behaved, it needs to satisfy the following conditions:

- (i) For the geometric sector, the metric potentials  $F$  and  $G$  should be free from coordinate and physical singularities within the interior region of the star  $0 \leq r \leq R$ , where the center (boundary) is at  $r = 0$  ( $r = R$ ) respectively.
- (ii) The metric potentials of the interior solution and the exterior<sup>11</sup> should match smoothly at the boundary.
- (iii) For the matter sector, the fluid density, radial and the tangential pressures should be free from coordinate or physical singularities within the interior region of the star. In addition, they should be maximum at the center of the star and monotonically decrease towards the boundary of the star. i.e.

---

<sup>11</sup>In our case the exterior solution is nothing rather Schwarzschild's one, since vacuum solutions of both GR and RT are equivalent.

## Physical conditions for a stellar model

- a.  $\rho(r=0) > 0$ ,  $\rho'(r=0) = 0$ ,  $\rho''(r=0) < 0$  and  $\rho'(0 < r \leq R) < 0$ ,
- b.  $p_r(r=0) > 0$ ,  $p_r'(r=0) = 0$ ,  $p_r''(r=0) < 0$  and  $p_r'(0 < r \leq R) < 0$ ,
- c.  $p_t(r=0) > 0$ ,  $p_t'(r=0) = 0$ ,  $p_t''(r=0) < 0$  and  $p_t'(0 < r \leq R) < 0$ .

(iv) At the center of the star ( $r=0$ ), the anisotropy parameter  $\Delta$  should vanish, i.e.  $p_r(r=0) = p_t(r=0)$ , and increasing toward the boundary, i.e.  $\Delta'(0 \leq r \leq R) > 0$ .

(v) At the boundary of the star ( $r=R$ ), the radial pressure should vanish, i.e.  $p_r(r=R) = 0$ . However, the tangential pressure at the boundary should not necessarily vanish.

# Physical conditions for a stellar model

(vi) Within the star ( $0 < r < R$ ), the density, radial and tangential pressures should be positive, i.e.  $\rho(0 < r < R) > 0$ ,  $p_r(0 < r < R) > 0$  and  $p_t(0 < r < R) > 0$ . (vii) The fluid density, radial and tangential pressures should fulfill the following energy conditions:

- a. Null energy condition (NEC):  $\rho c^2 + p_t > 0$ ,  $\rho > 0$ ,
- b. Weak energy condition (WEC):  $\rho c^2 + p_r > 0$ ,  $\rho > 0$ ,
- c. Dominant energy conditions (DEC):  $\rho c^2 \geq |p_r|$  and  $\rho c^2 \geq |p_t|$ ,
- d. Strong energy condition (SEC):  $\rho c^2 + p_r > 0$ ,  $\rho c^2 + p_t > 0$ ,  
 $\rho c^2 - p_r - 2p_t > 0$ .

## Physical conditions for a stellar model

(viii) The causality condition should be satisfied, that is the speed of sound should be smaller than unity everywhere inside the star and monotonically decrease toward the boundary, i.e. for the radial

velocity  $0 \leq v_r/c = \frac{1}{c} \sqrt{\frac{dp_r}{d\rho}} \leq 1$  and  $v_r'^2 < 0$ , and for the tangential

velocity  $0 \leq v_t/c = \frac{1}{c} \sqrt{\frac{dp_t}{d\rho}} \leq 1$  and  $v_t'^2 < 0$ .

(ix) The stability condition should be satisfied, i.e.

$-1 < (v_t^2 - v_r^2)/c^2 < 0$  within the star.

(x) The gravitational red-shift should be finite and positive everywhere inside the star and decreases monotonically toward the boundary, i.e.  $Z > 0$  and  $Z' < 0$ .

## Physical conditions for a stellar model

(xi) The adiabatic index stability condition for anisotropic star should be fulfilled, i.e. the adiabatic index  $\Gamma > \gamma$  where  $\gamma = 4/3$  is the adiabatic index corresponds to the isotropic case.

We note that the stellar model which fulfills the above mentioned conditions is physically viable and well behaved. In the following sections we are going to examine the model at hand with these conditions investigating possible roles of Rastall parameter.

# Physical properties of the model

## Non singular model

From Eqs. (16) and (19) one finds that the metric potentials at the center read

$$F(r=0) = \frac{(a_0 + 2a_1 a_2^2)^2}{16a_2^4} \quad \text{and} \quad G(r=0) = 1. \quad (25)$$

This ensures that the gravitational potentials are finite at the center of the star. Moreover, the derivatives of these potentials are finite at the center, i.e.  $F'(r=0) = G'(r=0) = 0$ . Equation (25) ensures that the metric is regular at the center.



# Physical properties of the model

## Non singular model

From Eqs. (20) one finds that the density, radial and tangential pressures at the center are

$$\begin{aligned}\rho(r=0) &= \frac{-12a_2^2[a_0(\epsilon-1) + 2a_1a_2^2(2\epsilon-1)]}{R^2(a_0 + 2a_1a_2^2)}, \\ p_r(r=0) = p_t(r=0) &= \frac{12a_2^2[a_0\epsilon + \frac{2}{3}a_1a_2^2(6\epsilon-1)]}{R^2(a_0 + 2a_1a_2^2)}.\end{aligned}\quad (26)$$

These ensure that the anisotropy parameter has a vanishing value at the center. Additionally, the Zeldovich condition states that the radial pressure must be less than or equal to the density at the center, i.e.  $\frac{p_r(0)}{\rho(0)} \leq 1$ , i.e.

$$\frac{-3(a_0 + 4a_1a_2^2)\epsilon + 2a_1a_2^2}{3(a_0 + 4a_1a_2^2)\epsilon - 3(a_0 + 2a_1a_2^2)} \leq 1.\quad (27)$$

# Physical properties of the model

## Non singular model

Using Eqs. (20) we give the derivative of energy density, radial and tangential pressures, respectively, as follows

$$\rho' = \frac{2ra_2^4}{R^8 (a_0 R^2 + 2a_1 a_2^2 R^2 - 2a_1 a_2^4 r^2)^2} \left\{ \begin{aligned} &216r^8 a_1^2 a_2^{12} \epsilon - 108r^8 a_1^2 a_2^{12} \\ &-676r^4 R^4 a_1^2 a_2^8 + 1352r^4 R^4 a_1^2 a_2^8 \epsilon - 168r^6 R^2 a_1 a_2^8 a_0 \epsilon \\ &+520r^4 R^4 a_1 a_2^6 a_0 \epsilon - 332r^4 R^4 a_1 a_2^6 a_0 - 120R^8 a_2^4 a_1^2 \\ &-27R^4 a_2^4 r^4 a_0^2 + 18R^4 a_2^4 r^4 a_0^2 \epsilon - 120a_0 R^8 a_2^2 a_1 + 192a_0 R^8 a_2^2 a_1 \epsilon \\ &+24a_0^2 R^8 \epsilon + 440r^6 R^2 a_1^2 a_2^{10} - 880r^6 R^2 a_1^2 a_2^{10} \epsilon + 56a_0^2 R^6 a_2^2 r^2 \\ &+108r^6 R^2 a_1 a_2^8 a_0 + 464r^2 R^6 a_1^2 a_2^6 - 928r^2 R^6 a_1^2 a_2^6 \epsilon \\ &+240R^8 a_2^4 a_1^2 \epsilon - 544r^6 R^6 a_2^4 r^2 a_0 a_1 \epsilon + 344R^6 a_2^4 r^2 a_0 a_1 \\ &-40a_0^2 R^6 a_2^2 r^2 \epsilon - 30a_0^2 R^8 \end{aligned} \right\}, \quad (28)$$

# Physical properties of the model

## Non singular model

$$p'_r = \frac{-2ra_2^4}{R^8 (a_0 R^2 + 2a_1 a_2^2 R^2 - 2a_1 a_2^4 r^2)^2} \left\{ \begin{aligned} &216 r^8 a_1^2 a_2^{12} \epsilon - 4 r^6 R^2 a_1 a_2^8 a_0 \\ &+ 1352 r^4 R^4 a_1^2 a_2^8 \epsilon - 100 r^4 R^4 a_1^2 a_2^8 - 168 r^6 R^2 a_1 a_2^8 a_0 \epsilon \\ &+ 520 r^4 R^4 a_1 a_2^6 a_0 \epsilon + 4 r^4 R^4 a_1 a_2^6 a_0 + 240 R^8 a_2^4 a_1^2 \epsilon \\ &+ 9 R^4 a_2^4 r^4 a_0^2 + 18 R^4 a_2^4 r^4 a_0^2 \epsilon - 8 a_0 R^8 a_2^2 a_1 + 192 a_0 R^8 a_2^2 a_1 \epsilon \\ &- 16 a_0^2 R^6 a_2^2 r^2 - 40 a_0^2 R^6 a_2^2 r^2 \epsilon + 6 a_0^2 R^8 \\ &+ 24 a_0^2 R^8 \epsilon - 12 r^8 a_1^2 a_2^{12} + 56 r^6 R^2 a_1^2 a_2^{10} - 880 r^6 R^2 a_1^2 a_2^{10} \epsilon \\ &- 24 R^8 a_2^4 a_1^2 - 544 R^6 a_2^4 r^2 a_0 a_1 \epsilon + 8 R^6 a_2^4 r^2 a_0 a_1 \\ &+ 80 r^2 R^6 a_1^2 a_2^6 - 928 r^2 R^6 a_1^2 a_2^6 \epsilon \end{aligned} \right\}, \quad (29)$$

# Physical properties of the model

## Non singular model

$$p'_t = \frac{-4ra_2^4}{R^8(a_0R^2 + 2a_1a_2^2R^2 - 2a_1a_2^4r^2)^2} \left\{ \begin{aligned} &108r^8a_1^2a_2^{12}\epsilon \\ &-24r^8a_1^2a_2^{12} + 96r^6R^2a_1^2a_2^{10} - 440r^6R^2a_1^2a_2^{10}\epsilon \\ &+ 676r^4R^4a_1^2a_2^8\epsilon - 84r^6R^2a_1a_2^8a_0\epsilon + 16r^6R^2a_1a_2^8a_0 \\ &- 464r^2R^6a_1^2a_2^6\epsilon + 96r^2R^6a_1^2a_2^6 + 260r^4R^4a_1a_2^6a_0\epsilon \\ &- 48r^4R^4a_1a_2^6a_0 - 24R^8a_2^4a_1^2 + 120R^8a_2^4a_1^2\epsilon \\ &- 272R^6a_2^4r^2a_0a_1\epsilon + 48R^6a_2^4r^2a_0a_1 + 9R^4a_2^4r^4a_0^2\epsilon \\ &+ 96a_0R^8a_2^2a_1\epsilon - 20a_0^2R^6a_2^2r^2\epsilon - 144r^4R^4a_1^2a_2^8 \\ &+ 12a_0^2R^8\epsilon - 16a_0R^8a_2^2a_1 \end{aligned} \right\}. \quad (30)$$

We use Eqs. (28)–(30) to show that the gradients of the energy-density, radial and tangential pressures are negative.

# Physical properties of the model

## Non singular model

The radial and tangential sound velocities are given

$$\begin{aligned} v_r^2 = \frac{dp_r}{d\rho} = & - \left\{ 216 r^8 a_1^2 a_2^{12} \epsilon - 12 r^8 a_1^2 a_2^{12} + 56 r^6 R^2 a_1^2 a_2^{10} - 880 r^6 R^2 a_1^2 a_2^{10} \epsilon + 1352 r^4 R^4 a_1^2 a_2^8 \epsilon \right. \\ & - 100 r^4 R^4 a_1^2 a_2^8 + 4 r^4 R^4 a_1 a_2^6 a_0 - 8 a_0 R^8 a_2^2 a_1 + 192 a_0 R^8 a_2^2 a_1 \epsilon - 16 a_0^2 R^6 a_2^2 r^2 \\ & - 168 r^6 R^2 a_1 a_2^8 a_0 \epsilon - 4 r^6 R^2 a_1 a_2^8 a_0 + 80 r^2 R^6 a_1^2 a_2^6 - 928 r^2 R^6 a_1^2 a_2^6 \epsilon + 520 r^4 R^4 a_1 a_2^6 a_0 \epsilon \\ & + 240 R^8 a_2^4 a_1^2 \epsilon - 24 R^8 a_2^4 a_1^2 - 544 R^6 a_2^4 r^2 a_0 a_1 \epsilon + 8 R^6 a_2^4 r^2 a_0 a_1 + 9 R^4 a_2^4 r^4 a_0^2 + 18 R^4 a_2^4 r^4 a_0^2 \epsilon \\ & - 40 a_0^2 R^6 a_2^2 r^2 \epsilon + 6 a_0^2 R^8 + 24 a_0^2 R^8 \epsilon \left. \right\} \left\{ 216 r^8 a_1^2 a_2^{12} \epsilon - 168 r^6 R^2 a_1 a_2^8 a_0 \epsilon - 120 R^8 a_2^4 a_1^2 \right. \\ & - 108 r^8 a_1^2 a_2^{12} + 440 r^6 R^2 a_1^2 a_2^{10} - 880 r^6 R^2 a_1^2 a_2^{10} \epsilon - 676 r^4 R^4 a_1^2 a_2^8 + 1352 r^4 R^4 a_1^2 a_2^8 \epsilon \\ & + 108 r^6 R^2 a_1 a_2^8 a_0 + 464 r^2 R^6 a_1^2 a_2^6 - 928 r^2 R^6 a_1^2 a_2^6 \epsilon + 520 r^4 R^4 a_1 a_2^6 a_0 \epsilon - 332 r^4 R^4 a_1 a_2^6 a_0 \\ & + 240 R^8 a_2^4 a_1^2 \epsilon - 544 R^6 a_2^4 r^2 a_0 a_1 \epsilon + 344 R^6 a_2^4 r^2 a_0 a_1 - 27 R^4 a_2^4 r^4 a_0^2 + 18 R^4 a_2^4 r^4 a_0^2 \epsilon \\ & \left. + 192 a_0 R^8 a_2^2 a_1 \epsilon + 56 a_0^2 R^6 a_2^2 r^2 - 40 a_0^2 R^6 a_2^2 r^2 \epsilon - 30 a_0^2 R^8 + 24 a_0^2 R^8 \epsilon - 120 a_0 R^8 a_2^2 a_1 \right\}^{-1}, \quad (31) \end{aligned}$$

# Physical properties of the model

## Non singular model

$$\begin{aligned} v_I^2 = \frac{dp_I}{d\rho} = & -2 \left\{ 108 r^8 a_1^2 a_2^{12} \epsilon - 24 r^8 a_1^2 a_2^{12} + 96 r^6 R^2 a_1^2 a_2^{10} - 440 r^6 R^2 a_1^2 a_2^{10} \epsilon + 676 r^4 R^4 a_1^2 a_2^8 \epsilon \right. \\ & - 144 r^4 R^4 a_1^2 a_2^8 - 48 r^4 R^4 a_1 a_2^6 a_0 + 96 a_0 R^8 a_2^2 a_1 \epsilon \\ & - 84 r^6 R^2 a_1 a_2^8 a_0 \epsilon + 16 r^6 R^2 a_1 a_2^8 a_0 - 464 r^2 R^6 a_1^2 a_2^6 \epsilon + 96 r^2 R^6 a_1^2 a_2^6 + 260 r^4 R^4 a_1 a_2^6 a_0 \epsilon \\ & - 24 R^8 a_2^4 a_1^2 + 120 R^8 a_2^4 a_1^2 \epsilon - 272 R^6 a_2^4 r^2 a_0 a_1 \epsilon + 48 R^6 a_2^4 r^2 a_0 a_1 + 9 R^4 a_2^4 r^4 a_0^2 \epsilon - 16 a_0 R^8 a_2^2 a_1 \\ & - 20 a_0^2 R^6 a_2^2 r^2 \epsilon + 12 a_0^2 R^8 \epsilon \left. \right\} \left\{ -108 r^8 a_1^2 a_2^{12} + 216 r^8 a_1^2 a_2^{12} \epsilon + 440 r^6 R^2 a_1^2 a_2^{10} - 880 r^6 R^2 a_1^2 a_2^{10} \epsilon \right. \\ & - 676 r^4 R^4 a_1^2 a_2^8 + 520 r^4 R^4 a_1 a_2^6 a_0 \epsilon - 27 R^4 a_2^4 r^4 a_0^2 + 24 a_0^2 R^8 \epsilon - 30 a_0^2 R^8 \\ & + 1352 r^4 R^4 a_1^2 a_2^8 \epsilon - 168 r^6 R^2 a_1 a_2^8 a_0 \epsilon + 108 r^6 R^2 a_1 a_2^8 a_0 + 464 r^2 R^6 a_1^2 a_2^6 - 928 r^2 R^6 a_1^2 a_2^6 \epsilon \\ & - 332 r^4 R^4 a_1 a_2^6 a_0 - 120 R^8 a_2^4 a_1^2 + 240 R^8 a_2^4 a_1^2 \epsilon - 544 R^6 a_2^4 r^2 a_0 a_1 \epsilon + 344 R^6 a_2^4 r^2 a_0 a_1 \\ & \left. + 18 R^4 a_2^4 r^4 a_0^2 \epsilon - 120 a_0 R^8 a_2^2 a_1 + 192 a_0 R^8 a_2^2 a_1 \epsilon + 56 a_0^2 R^6 a_2^2 r^2 - 40 a_0^2 R^6 a_2^2 r^2 \epsilon \right\}^{-1}. \quad (32) \end{aligned}$$

We use Eqs. (31) and (32) to show that the sound speeds satisfy the causality and the stability conditions.

# Physical properties of the model

## Matching conditions

We note that the exterior spacetime of a static spherically symmetric star is the same for both GR and RT, since the exterior region is vacuum. Thus no reason to expect any solution rather the exterior Schwarzschild one for Rastall's theory, that is

$$ds^2 = -\left(1 - \frac{2M}{r}\right)dt^2 + \left(1 - \frac{2M}{r}\right)^{-1} dr^2 + r^2(d\theta^2 + d\phi^2), \quad (33)$$

where  $M$  is the total mass  $r > 2M$ . We are going to match the interior spacetime metrics (16) and (19) and the exterior Schwarzschild spacetime metric (33) at the boundary of the star  $r = R$ . Therefore, the continuity of the metric functions, as stated by condition (ii), across the boundary gives the conditions

$$F(r = R) = \frac{[a_0 - 2a_1 a_2^2 (a^2 - 1)]^2}{12a_2^4 (a^2 - 1)^2} = \left(1 - \frac{2M}{R}\right),$$
$$G(r = R) = (a_2^2 - 1)^4 = \left(1 - \frac{2M}{R}\right). \quad (34)$$

# Physical properties of the model

## Matching conditions

In addition, the radial pressure (20) approaches zero at the star boundary,  $p_{r|r=R} = 0$ , which reads

$$\begin{aligned} & 2a_1 a_0^{10} - 10a_1 a_0^8 + (20a_1 + 3a_0)a_0^6 - 4(5a_1 + 2a_0)a_0^4 + 2(4a_1 + 3a_0)a_0^2 \\ - & \left[ 36a_1 a_2^{10} - 148a_1 a_2^8 + 2(116a_1 - 3a_0)a_2^6 - 4(42a_1 - 5a_0)a_2^4 \right. \\ & \left. + 24(2a_1 - a_0)a_2^2 - 12a_0 \right] \epsilon = 0 \end{aligned} \quad (35)$$

The above constraint ensures that condition (v) is fulfilled. From the above conditions, namely (34) and (35), we get the constraints on the set of constants  $\{a_0, a_1, a_2\}$  in terms of the star mass  $M$ , radius  $R$  in addition to the Rastall parameter  $\epsilon$ . Using observational pulsars data, knowing the observed values of  $M$  and  $R$ , we obtain the corresponding numerical values for a particular choice of  $\epsilon$ .



## Astrophysical observational constraints

We use the observational constraints of the particular pulsar *Her X-1*, whose mass  $M = 0.85 \pm 0.15 M_{\odot}$  and radius  $R = 8.1 \pm 0.41 \text{ km}^{12}$ , where  $M_{\odot}$  ( $= 1.989 \times 10^{30} \text{ kg}$ ) denotes the solar mass. Then, the boundary conditions (34) and (35) are adopted to determine the dimensionless constants in terms of the Rastall parameter  $\epsilon$

$$a_0 = \frac{2.564\epsilon - 0.4694}{4.542\epsilon - 1.514}, a_1 = -6.192 a_0 + 1.661 \text{ and } a_2 = 0.298.$$

Noting that we select  $a_2 < 1$  which is required by the regularity condition of ansatz (16).

---

<sup>12</sup>T. Gangopadhyay, S. Ray, X.D. Li, J. Dey, M. Dey, Mon. Not. Roy. Astron. Soc. **431**, 3216 (2013)

# Astrophysical observational constraints

Substituting the above expressions into Zeldovich condition (27), keeping in mind that the RT predictions are not expected to be far from GR ones (i.e.  $\epsilon$  should be small), we obtain the following constraints on Rastall parameter  $-1.880 \lesssim \epsilon \lesssim 0.259$ .

# Astrophysical observational constraints

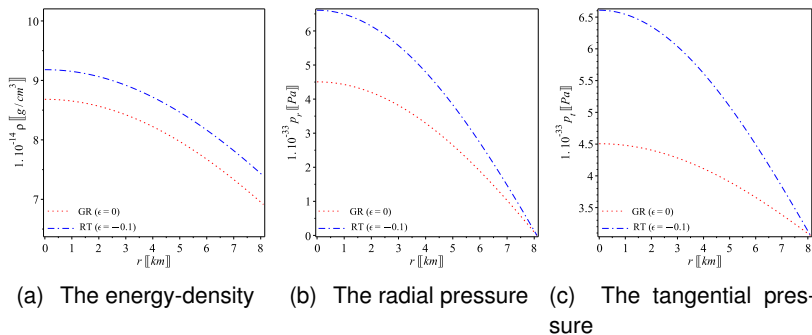


**Figure:** Plots of the density, radial and tangential pressures given by (20) versus the radial coordinate  $r$  in km of the pulsar *Her X-1* ( $M = 0.85 \pm 0.15 M_{\odot}$ ,  $R = 8.1 \pm 0.41$  km). We set  $\epsilon = -0.1$ ,  $a_0 \approx 0.369$ ,  $a_1 \approx -0.622$  and  $a_2 \approx 0.298$ .

# Astrophysical observational constraints

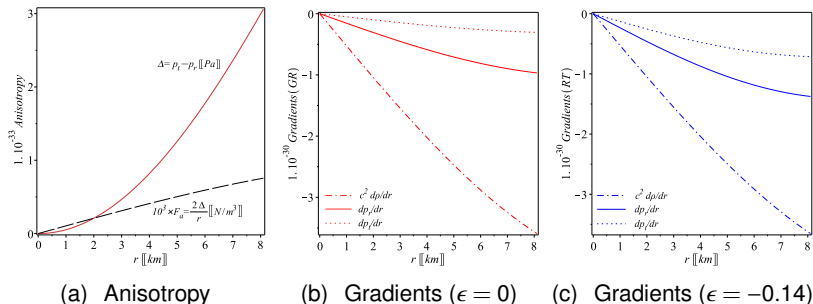
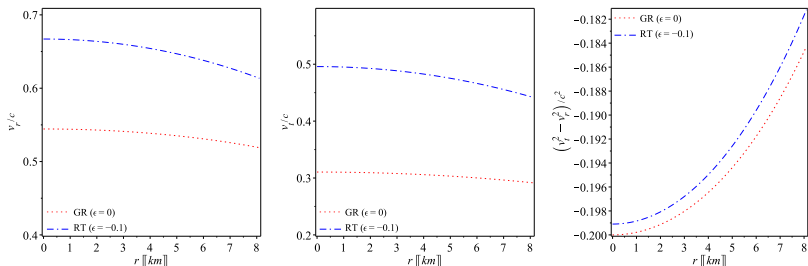


**Figure:** Plot of the anisotropy parameter (18), anisotropic force  $F_a = 2\Delta/r$ . We note that the Rastall parameter has no contribution in the anisotropy, therefore GR and RT predicts same anisotropy in the case of spherical symmetry as discussed after (15). For  $\epsilon = 0$  and  $\epsilon \neq 0$ , the gradients of the density, tangential and radial pressures given by Eqs. (28)–(30) versus the radial coordinate  $r$  in km of the pulsar *Her X-1*.

# Astrophysical observational constraints



(a) Radial speed of sound (b) Tangential speed of sound (c) difference between radial and tangential speed of sounds

**Figure:** The radial and tangential sound speeds (29) versus the radial coordinate  $r$  in km for the pulsar *Her X-1*. The plots confirm that the model fulfill the causality and the stability conditions (viii) and (ix).

# Astrophysical observational constraints

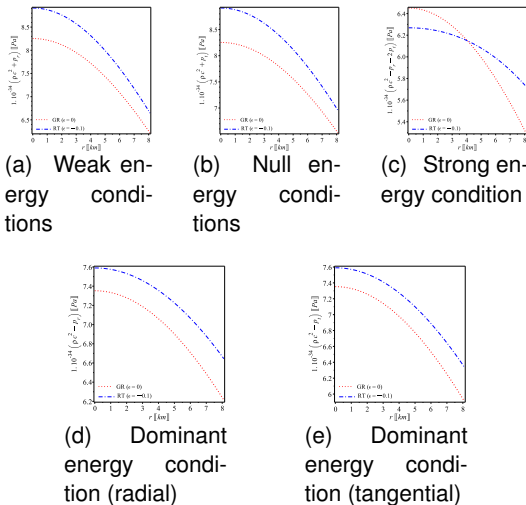
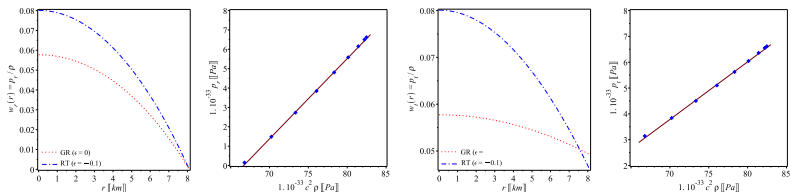


**Figure:** The weak, null, strong and dominant energy conditions, using Eqs. (20), versus the radial coordinate  $r$  in km for the pulsar *Her X-1*. The plots show that the model fulfill the energy conditions (vii).

# Astrophysical observational constraints



(a) radial EoS (b) linear radial EoS (c) tangential EoS (d) linear tangential EoS

**Figure:** Figs. (a) and (a) show the behaviours of the EoS parameters, defined as  $w_r(r) = p_r/\rho$  and  $w_t(r) = p_t/\rho$ , at different radial distances within the pulsar *Her X-1* as predicted by RT and GR. We note that no EoS are imposed at any stage of the present work, while it is evidently that the result fit well with the linear behaviour whereas the best fit lines in Fig. (b) and (d) are given by  $p_r = 0.414\rho - 27.6$  and  $p_t = 0.223\rho - 11.8$  in RT case.

# Astrophysical observational constraints

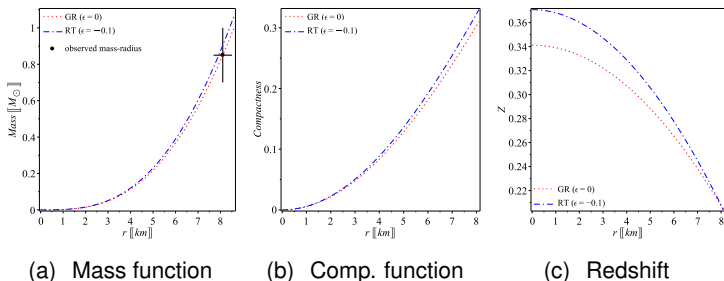


**Figure:** The mass function plot confirms the agreement with observational data. The plot shows that RT predicts compactness values higher than GR. The redshift is finite everywhere within the pulsar and decreases toward the surface as stated by condition (x) and also predict a surface redshift consistent with the upper limit constraints as given by.



# Stability of the model

## Equilibrium analysis via Tolman-Oppenheimer-Volkoff equation

We assume hydrostatic equilibrium to be everywhere within the stable compact star. This configuration, then, can be described by the GR based TOV equation which gives the following stability constraint

$$\frac{2(p_t - p_r)}{r} - \frac{M_g(\rho + p_r) \sqrt{F}}{r \sqrt{G}} - \frac{dp_r}{dr} = 0, \quad (36)$$

where  $M = M_g(r)$  is the gravitational mass within a radius  $r$ , which is defined by the Tolman-Whittaker mass formula

$$M_g(r) = 4\pi \int_0^r \left( T_t^t - T_r^r - T_\theta^\theta - T_\phi^\phi \right) r^2 \sqrt{FG} dr = \frac{rF' \sqrt{G}}{2F \sqrt{F}}. \quad (37)$$

# Stability of the model

## Equilibrium analysis via Tolman-Oppenheimer-Volkoff equation

Inserting Eq. (37) into (36), we get

$$\frac{2}{r}(p_t - p_r) - \frac{F'}{2F}(\rho + p_r) - \frac{dp_r}{dr} = F_a + F_g + F_h = 0, \quad (38)$$

where  $F_g = -\frac{F'}{2F}(\rho + p_r)$  and  $F_h = -\frac{dp_r}{dr}$  are the gravitational and the hydrostatic forces respectively, in addition to the anisotropic force  $F_a$ . We note that the TOV equation should be modified in RT due to the non-minimal coupling constraint,  $\mathcal{T}^\alpha{}_{\beta;\alpha} = \epsilon \partial_\beta \mathcal{R}$ , to include one more force  $F_R$  as following

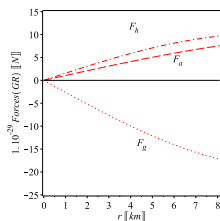
$$F_a + F_g + F_h + F_R = 0, \quad (39)$$

where  $F_R = -\frac{\epsilon}{1-4\epsilon} \frac{d}{dr}(\rho - p_r - 2p_t)$ . These different forces, for GR ( $\epsilon = 0$ ) and RT ( $\epsilon \neq 0$ ), are plotted in Fig. 7 using the pulsar *Her X-1* data.

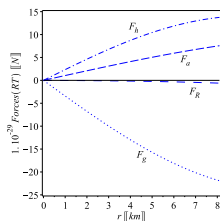
# Stability of the model

## Equilibrium analysis via Tolman-Oppenheimer-Volkoff equation

In conclusion, we verify the stability of the model via TOV equation using the pulsar *Her X-1* data.



(a) TOV equation  
( $\epsilon = 0$ )



(b) TOV equation  
( $\epsilon = -0.1$ )

**Figure:** Plots of the forces of TOV equation (38) in cases  $\epsilon = 0$  and  $\epsilon = -0.1$  versus the radius  $r$  using the constants constrained from *Her X-1*. In the RT case the negative gravitational force is the dominant one over the hydrostatic and the anisotropic forces. This guarantees stable equilibrium configuration for the pulsar.

# Stability of the model

## Relativistic adiabatic indices

Another verification of the stable equilibrium configuration of a spherically symmetric object can be done via the adiabatic index, that is defined as the ratio of two specific heats and can be given as follows

$$\Gamma = \frac{\rho + p_r}{\rho_r} v_r^2. \quad (40)$$

For the general case of anisotropic spheroid fluid, it has been shown that the object is in a neutral equilibrium if its adiabatic index  $\Gamma = \gamma$  and in a stable equilibrium if  $\Gamma > \gamma$ <sup>13</sup>, whereas

$$\gamma = \frac{4}{3} \left( 1 + \frac{F_a}{2|\rho'_r|} \right)_{max}. \quad (41)$$

---


<sup>13</sup>R. Chan, L. Herrera, N.O. Santos, Monthly Notices of the Royal Astronomical Society **265**(3), 533 (1993)

# Stability of the model

## Relativistic adiabatic indices

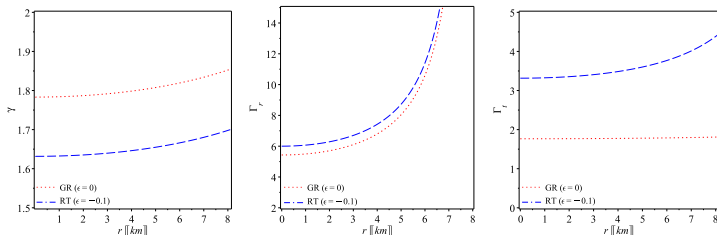
Clearly, for an isotropic fluid, the object is in a neutral equilibrium if the adiabatic index  $\Gamma = \frac{4}{3}$ , while for  $\Gamma > \frac{4}{3}$  the object is in a stable equilibrium<sup>14</sup>. Using Eq. (41), we get

$$\begin{aligned} \gamma = & \frac{2}{3R^8} \left[ \left( 2R^8 \left| \frac{ra_2^4}{R^8 (a_0 R^2 + 2a_1 a_2^2 R^2 - 2a_1 a_2^4 r^2)^2} \right\{ 216r^8 a_1^2 a_2^{12} \epsilon - 12r^8 a_1^2 a_2^{12} + 56r^6 R^2 a_1^2 a_2^{10} \right. \right. \\ & + 1352r^4 R^4 a_1^2 a_2^8 \epsilon - 100r^4 R^4 a_1^2 a_2^8 - 168r^6 R^2 a_1 a_2^8 a_0 \epsilon - 4r^6 R^2 a_1 a_2^8 a_0 + 80r^2 R^6 a_1^2 a_2^6 - 928r^2 R^6 a_1^2 a_2^6 \epsilon \\ & + 520r^4 R^4 a_1 a_2^6 a_0 \epsilon + 18R^4 a_2^4 r^4 a_0^2 \epsilon + 24a_0^2 R^8 \epsilon - 40a_0^2 R^6 a_2^2 r^2 \epsilon + 6a_0^2 R^8 - 880r^6 R^2 a_1^2 a_2^{10} \epsilon \\ & + 4r^4 R^4 a_1 a_2^6 a_0 + 240R^8 a_2^4 a_1^2 \epsilon - 24R^8 a_2^4 a_1^2 - 544R^6 a_2^4 r^2 a_0 a_1 \epsilon + 8R^6 a_2^4 r^2 a_0 a_1 + 9R^4 a_2^4 r^4 a_0^2 \\ & \left. \left. - 8a_0 R^8 a_2^2 a_1 + 192a_0 R^8 a_2^2 a_1 \epsilon - 16a_0^2 R^6 a_2^2 r^2 \right\} + 6R^4 r a_2^4 - 8R^2 r^3 a_2^6 + 3a_2^8 r^5 \right) \\ & \left\{ R^8 \left[ a_0 R^2 + 2a_1 a_2^2 R^2 - 2a_1 a_2^4 r^2 \right]^2 \right\} \left\{ r a_2^4 \left( 216r^8 a_1^2 a_2^{12} \epsilon - 12r^8 a_1^2 a_2^{12} + 56r^6 R^2 a_1^2 a_2^{10} - 880r^6 R^2 a_1^2 a_2^{10} \epsilon \right. \right. \\ & + 1352r^4 R^4 a_1^2 a_2^8 \epsilon - 100r^4 R^4 a_1^2 a_2^8 - 168r^6 R^2 a_1 a_2^8 a_0 \epsilon - 4r^6 R^2 a_1 a_2^8 a_0 + 80r^2 R^6 a_1^2 a_2^6 - 928r^2 R^6 a_1^2 a_2^6 \epsilon \\ & + 4r^4 R^4 a_1 a_2^6 a_0 + 240R^8 a_2^4 a_1^2 \epsilon - 24R^8 a_2^4 a_1^2 - 544R^6 a_2^4 r^2 a_0 a_1 \epsilon + 8R^6 a_2^4 r^2 a_0 a_1 + 9R^4 a_2^4 r^4 a_0^2 + 18R^4 a_2^4 r^4 a_0^2 \epsilon \\ & \left. \left. - 8a_0 R^8 a_2^2 a_1 + 192a_0 R^8 a_2^2 a_1 \epsilon - 16a_0^2 R^6 a_2^2 r^2 - 40a_0^2 R^6 a_2^2 r^2 \epsilon + 6a_0^2 R^8 + 24a_0^2 R^8 \epsilon + 520r^4 R^4 a_1 a_2^6 a_0 \epsilon \right) \right\}^{-1} \end{aligned}$$

<sup>14</sup>H. Heintzmann, W. Hillebrandt, *aap* **38**(1), 51 (1975) 

# Stability of the model

## Relativistic adiabatic indices



(a)  $\gamma$  in cases  $\epsilon = 0$  and  $\epsilon \neq 0$  (b)  $\Gamma_r$  in cases  $\epsilon = 0$  and  $\epsilon \neq 0$  (c)  $\Gamma_t$  in cases  $\epsilon = 0$  and  $\epsilon \neq 0$

**Figure:** Plots of the Adiabatic indices  $\gamma$ ,  $\Gamma_r$  and  $\Gamma_t$ , namely (42)–(44), versus the radius  $r$  using the constants constrained from *Her X-1*. For RT, the adiabatic index  $\gamma$  less than the GR case but still greater than the neutral equilibrium value  $\gamma = \frac{4}{3}$ . The radial and tangential adiabatic indices have higher values whereas the stability constraints  $\Gamma_r > \gamma$  and  $\Gamma_t > \gamma$  are fulfilled everywhere within the pulsar.

# Stability of the model

## Relativistic adiabatic indices

From Eq. (40), we obtain the adiabatic index of solution (20) in the form

$$\begin{aligned}
 \Gamma_r = & -4 \left\{ (4a_1 a_2^2 R^2 + 3a_0 R^2 - 4a_1 a_2^4 r^2) (R^2 - a_2^2 r^2)^3 \left[ 216r^8 a_1^2 a_2^{12} \epsilon - 12r^8 a_1^2 a_2^{12} + 56r^6 R^2 a_1^2 a_2^{10} - 880r^6 R^2 a_1^2 a_2^{10} \right. \right. \\
 & a_2^{10} \epsilon + 1352r^4 R^4 a_1^2 a_2^8 \epsilon - 100r^4 R^4 a_1^2 a_2^8 - 168r^6 R^2 a_1 a_2^8 a_0 \epsilon - 4r^6 R^2 a_1 a_2^8 a_0 + 80r^2 R^6 a_1^2 a_2^6 - 928r^2 R^6 a_1^2 a_2^6 \epsilon \\
 & + 520r^4 R^4 a_1 a_2^6 a_0 \epsilon + 4r^4 R^4 a_1 a_2^6 a_0 + 240R^8 a_2^4 a_1^2 \epsilon - 24R^8 a_2^4 a_1^2 - 544R^6 a_2^4 r^2 a_0 a_1 \epsilon + 8R^6 a_2^4 r^2 a_0 a_1 \\
 & + 9R^4 a_2^4 r^4 a_0^2 + 18R^4 a_2^4 r^4 a_0^2 \epsilon - 8a_0 R^8 a_2^2 a_1 + 192a_0 R^8 a_2^2 a_1 \epsilon - 16a_0^2 R^6 a_2^2 r^2 - 40a_0^2 R^6 a_2^2 r^2 \epsilon + 6a_0^2 R^8 \\
 & \left. + 24a_0^2 R^8 \epsilon \right\} \left\{ \left[ 36a_1 r^8 a_2^{10} \epsilon - 2a_1 r^8 a_2^{10} + 10r^6 R^2 a_1 a_2^8 - 148r^6 R^2 a_1 a_2^8 \epsilon - 20r^4 R^4 a_1 a_2^6 + 232R^4 r^4 a_2^6 a_1 \epsilon \right. \right. \\
 & - 3R^2 r^6 a_2^6 a_0 - 6R^2 r^6 a_2^6 a_0 \epsilon + 20R^6 r^2 a_2^4 a_1 - 168R^6 r^2 a_2^4 a_1 \epsilon + 8R^4 r^4 a_2^4 a_0 + 20R^4 r^4 a_2^4 a_0 \epsilon - 8R^8 a_2^2 a_1 \\
 & \left. + 48R^8 a_2^2 a_1 \epsilon - 6R^6 a_2^2 r^2 a_0 - 24R^6 a_2^2 r^2 a_0 \epsilon + 12\epsilon R^8 a_0 \right] \left[ 216r^8 a_1^2 a_2^{12} \epsilon - 108r^8 a_1^2 a_2^{12} + 440r^6 R^2 a_1^2 a_2^{10} \right. \\
 & - 880r^6 R^2 a_1^2 a_2^{10} \epsilon - 676r^4 R^4 a_1^2 a_2^8 + 1352r^4 R^4 a_1^2 a_2^8 \epsilon - 168r^6 R^2 a_1 a_2^8 a_0 \epsilon + 108r^6 R^2 a_1 a_2^8 a_0 + 464r^2 R^6 a_1^2 a_2^6 \\
 & - 928r^2 R^6 a_1^2 a_2^6 \epsilon + 520r^4 R^4 a_1 a_2^6 a_0 \epsilon - 332r^4 R^4 a_1 a_2^6 a_0 - 120R^8 a_2^4 a_1^2 + 240R^8 a_2^4 a_1^2 \epsilon - 544R^6 a_2^4 r^2 a_0 a_1 \epsilon \\
 & \left. + 344R^6 a_2^4 r^2 a_0 a_1 - 27R^4 a_2^4 r^4 a_0^2 + 18R^4 a_2^4 r^4 a_0^2 \epsilon - 120a_0 R^8 a_2^2 a_1 + 192a_0 R^8 a_2^2 a_1 \epsilon + 56a_0^2 R^6 a_2^2 r^2 \right. \\
 & \left. \left. - 40a_0^2 R^6 a_2^2 r^2 \epsilon - 30a_0^2 R^8 + 24a_0^2 R^8 \epsilon \right] \right\}^{-1}, \tag{43}
 \end{aligned}$$

# Stability of the model

## Relativistic adiabatic indices

and

$$\begin{aligned}
 \Gamma_t = - & \left\{ \left[ 108 r^8 a_1^2 a_2^{12} \epsilon - 24 r^8 a_1^2 a_2^{12} + 96 r^6 R^2 a_1^2 a_2^{10} - 440 r^6 R^2 a_1^2 a_2^{10} \epsilon + 676 r^4 R^4 a_1^2 a_2^8 \epsilon - 144 r^4 R^4 a_1^2 a_2^8 \right. \right. \\
 & - 84 r^6 R^2 a_1 a_2^8 a_0 \epsilon + 16 r^6 R^2 a_1 a_2^8 a_0 - 464 r^2 R^6 a_1^2 a_2^6 \epsilon + 96 r^2 R^6 a_1^2 a_2^6 + 260 r^4 R^4 a_1 a_2^6 a_0 \epsilon - 48 r^4 R^4 a_1 a_2^6 a_0 \\
 & - 24 R^8 a_2^4 a_1^2 + 120 R^8 a_2^4 a_1^2 \epsilon - 272 R^6 a_2^4 r^2 a_0 a_1 \epsilon + 48 R^6 a_2^4 r^2 a_0 a_1 + 9 R^4 a_2^4 r^4 a_0^2 \epsilon - 16 a_0 R^8 a_2^2 a_1 + 12 a_0^2 R^8 \epsilon \\
 & \left. \left. + 96 a_0 R^8 a_2^2 a_1 \epsilon - 20 a_0^2 R^6 a_2^2 r^2 \epsilon \right] \left[ 10 a_1 r^8 a_2^{10} - 42 r^6 R^2 a_1 a_2^8 - 9 R^2 r^6 a_2^6 a_0 + 68 r^4 R^4 a_1 a_2^6 + 28 R^4 r^4 a_2^4 a_0 \right. \right. \\
 & \left. \left. - 52 R^6 r^2 a_2^4 a_1 - 30 R^6 a_2^2 r^2 a_0 + 16 R^8 a_2^2 a_1 + 12 a_0 R^8 \right] \right\} \left\{ \left[ 18 a_1 r^8 a_2^{10} \epsilon - 4 a_1 r^8 a_2^{10} - 74 r^6 R^2 a_1 a_2^8 \epsilon + 16 r^6 R^2 a_1 a_2^8 \right. \right. \\
 & \left. \left. + 116 R^4 r^4 a_2^6 a_1 \epsilon - 24 r^4 R^4 a_1 a_2^6 - 3 R^2 r^6 a_2^6 a_0 \epsilon - 84 R^6 r^2 a_2^4 a_1 \epsilon + 16 R^6 r^2 a_2^4 a_1 + 10 R^4 r^4 a_2^4 a_0 \epsilon - 4 R^8 a_2^2 a_1 \right. \right. \\
 & \left. \left. + 24 R^8 a_2^2 a_1 \epsilon - 12 R^6 a_2^2 r^2 a_0 \epsilon + 6 \epsilon R^8 a_0 \right] \left[ 216 r^8 a_1^2 a_2^{12} \epsilon - 108 r^8 a_1^2 a_2^{12} + 440 r^6 R^2 a_1^2 a_2^{10} - 880 r^6 R^2 a_1^2 a_2^{10} \epsilon \right. \right. \\
 & - 676 r^4 R^4 a_1^2 a_2^8 + 1352 r^4 R^4 a_1^2 a_2^8 \epsilon - 168 r^6 R^2 a_1 a_2^8 a_0 \epsilon + 108 r^6 R^2 a_1 a_2^8 a_0 + 464 r^2 R^6 a_1^2 a_2^6 - 928 r^2 R^6 a_1^2 a_2^6 \epsilon \\
 & + 520 r^4 R^4 a_1 a_2^6 a_0 \epsilon - 332 r^4 R^4 a_1 a_2^6 a_0 - 120 R^8 a_2^4 a_1^2 + 240 R^8 a_2^4 a_1^2 \epsilon - 544 R^6 a_2^4 r^2 a_0 a_1 \epsilon + 344 R^6 a_2^4 r^2 a_0 a_1 \\
 & \left. \left. - 27 R^4 a_2^4 r^4 a_0^2 + 18 R^4 a_2^4 r^4 a_0^2 \epsilon - 120 a_0 R^8 a_2^2 a_1 + 192 a_0 R^8 a_2^2 a_1 \epsilon + 56 a_0^2 R^6 a_2^2 r^2 - 40 a_0^2 R^6 a_2^2 r^2 \epsilon \right. \right. \\
 & \left. \left. - 30 a_0^2 R^8 + 24 a_0^2 R^8 \epsilon \right] \right\}. \tag{44}
 \end{aligned}$$



# More Observational Constraints

## Pulsars' data

Table 1: Observed mass-radius of twenty pulsars and the corresponding model parameters ( $\epsilon = -0.1$ ).

Pulsar	obs. mass ( $M_{\odot}$ )	obs. radius [km]	est. mass ( $M_{\odot}$ )	$a_0$	$a_1$	$a_2$
Her X-1	$0.85 \pm 0.15$	$8.1 \pm 0.41$	0.905	0.369	-0.622	0.298
RX J185635-3754	$0.9 \pm 0.2$	6	0.949	0.517	-0.706	0.369
LMC X-4	$1.04 \pm 0.09$	$8.301 \pm 0.2$	1.103	0.375	-0.658	0.330
GW170817-2	$1.27 \pm 0.09$	$11.9 \pm 1.4$	1.351	0.437	-0.625	0.301
EXO 1785-248	$1.3 \pm 0.2$	$8.849 \pm 0.4$	1.372	0.507	-0.699	0.364
PSR J0740+6620	$1.34 \pm 0.16$	$12.71 \pm 1.19$	1.426	0.370	-0.623	0.298
M13	$1.38 \pm 0.2$	$9.95 \pm 0.27$	1.459	0.481	-0.683	0.351
LIGO	1.4	$12.9 \pm 0.8$	1.489	0.381	-0.628	0.303
X7	1.4	$14.5 \pm 1.8$	1.492	0.340	-0.607	0.284
PSR J0037-4715	$1.44 \pm 0.07$	$13.6 \pm 0.9$	1.532	0.372	-0.623	0.299
PSR J0740+6620	$1.44 \pm 0.16$	$13.02 \pm 1.24$	1.531	0.388	-0.632	0.307
GW170817-1	$1.45 \pm 0.09$	$11.9 \pm 1.4$	1.539	0.425	-0.652	0.325
4U 1820-30	$1.46 \pm 0.2$	$11.1 \pm 1.8$	1.546	0.457	-0.670	0.440
Cen X-3	$1.49 \pm 0.49$	$9.178 \pm 0.13$	1.566	0.556	-0.731	0.388
4U 1608-52	$1.57 \pm 0.3$	$9.8 \pm 1.8$	1.651	0.550	-0.727	0.385
KS 1731-260	$1.61 \pm 0.37$	$10 \pm 2.2$	1.692	0.552	-0.728	0.386
EXO 1745-268	$1.65 \pm 0.25$	$10.5 \pm 1.8$	1.736	0.540	-0.720	0.380
Vela X-1	$1.77 \pm 0.08$	$9.56 \pm 0.08$	1.845	0.627	-0.781	0.424
4U 1724-207	$1.81 \pm 0.27$	$12.2 \pm 1.4$	1.909	0.512	-0.702	0.366
SAX J1748.9-2021	$1.81 \pm 0.3$	$11.7 \pm 1.7$	1.906	0.532	-0.715	0.376
PSR J1614-2230 <sup>15</sup>	$1.97 \pm 0.04$	$13 \pm 2$	2.076	0.522	-0.709	0.371
PSR J0348+0432	$2.01 \pm 0.04$	$13 \pm 2$	2.117	0.532	-0.715	0.376

<sup>15</sup>We note that the estimated mass for massive pulsars slightly exceeds the observational value which would impose more strict constraints on Rastall parameter to be  $\epsilon = 0.06$ .

# More Observational Constraints

## Pulsars' data

Table 2: Calculated physical quantities of the most interest.

Pulsar	$\rho(0)$ [g/cm <sup>3</sup> ]	$\rho_R$ [g/cm <sup>3</sup> ]	$\frac{v_r^2(0)}{c^2}$	$\frac{v_r^2(R)}{c^2}$	$v_r^2(0)^2$	$v_r^2(R)^2$	$\rho c^2 - p_r - 2p_t _0$ [Pa]	$\rho - p_r - 2p_t _R$ [Pa]	$Z_R$
Her X-1	$9.18 \times 10^{14}$	$7.39 \times 10^{14}$	0.445	0.376	0.246	0.195	$6.27 \times 10^{34}$	$5.73 \times 10^{34}$	0.204
RX J185635-3754	$2.53 \times 10^{15}$	$1.81 \times 10^{15}$	0.608	0.451	0.402	0.276	$1.25 \times 10^{35}$	$1.26 \times 10^{35}$	0.340
LMC X-4	$1.07 \times 10^{15}$	$8.19 \times 10^{14}$	0.506	0.406	0.304	0.228	$6.53 \times 10^{34}$	$6.08 \times 10^{34}$	0.260
GW170817-2	$4.33 \times 10^{14}$	$3.48 \times 10^{14}$	0.450	0.379	0.250	0.198	$2.93 \times 10^{34}$	$2.68 \times 10^{34}$	0.208
EXO 1785-248	$1.13 \times 10^{15}$	$8.21 \times 10^{14}$	0.593	0.444	0.388	0.269	$5.80 \times 10^{34}$	$5.76 \times 10^{34}$	0.329
PSR J0740+6620	$3.75 \times 10^{14}$	$3.01 \times 10^{14}$	0.446	0.377	0.247	0.196	$2.55 \times 10^{34}$	$2.33 \times 10^{34}$	0.205
M13	$8.39 \times 10^{14}$	$6.20 \times 10^{14}$	0.556	0.429	0.353	0.253	$4.63 \times 10^{34}$	$4.45 \times 10^{34}$	0.302
LIGO	$3.76 \times 10^{14}$	$3.00 \times 10^{14}$	0.454	0.381	0.255	0.201	$2.52 \times 10^{34}$	$2.31 \times 10^{34}$	0.213
X7	$2.61 \times 10^{14}$	$2.14 \times 10^{14}$	0.424	0.366	0.226	0.183	$1.85 \times 10^{34}$	$1.69 \times 10^{34}$	0.183
PSR J0037-4715	$3.29 \times 10^{14}$	$2.64 \times 10^{14}$	0.447	0.378	0.248	0.197	$2.24 \times 10^{34}$	$2.04 \times 10^{34}$	0.206
PSR J0740+6620	$3.77 \times 10^{14}$	$2.99 \times 10^{14}$	0.460	0.384	0.260	0.204	$2.50 \times 10^{34}$	$2.29 \times 10^{34}$	0.219
GW170817-1	$5.04 \times 10^{14}$	$3.89 \times 10^{14}$	0.494	0.401	0.293	0.222	$3.14 \times 10^{34}$	$2.91 \times 10^{34}$	0.250
4U 1820-30	$6.33 \times 10^{14}$	$4.77 \times 10^{14}$	0.528	0.416	0.325	0.239	$3.70 \times 10^{34}$	$3.49 \times 10^{34}$	0.279
Cent X-3	$1.19 \times 10^{15}$	$8.24 \times 10^{14}$	0.677	0.477	0.469	0.305	$4.98 \times 10^{34}$	$5.51 \times 10^{34}$	0.386
4U 1608-52	$1.03 \times 10^{15}$	$7.15 \times 10^{14}$	0.664	0.472	0.456	0.300	$4.45 \times 10^{34}$	$4.82 \times 10^{34}$	0.378
KS 1731-260	$9.92 \times 10^{14}$	$6.89 \times 10^{14}$	0.669	0.474	0.461	0.302	$4.24 \times 10^{34}$	$4.63 \times 10^{34}$	0.381
EXO 1745-268	$8.74 \times 10^{14}$	$6.14 \times 10^{14}$	0.646	0.466	0.439	0.293	$3.95 \times 10^{34}$	$4.18 \times 10^{34}$	0.366
Vela X-1	$1.29 \times 10^{15}$	$8.33 \times 10^{14}$	0.861	0.538	0.645	0.371	$3.01 \times 10^{34}$	$5.11 \times 10^{34}$	0.486
4U 1724-207	$6.04 \times 10^{14}$	$4.35 \times 10^{14}$	0.600	0.447	0.394	0.273	$3.04 \times 10^{34}$	$3.04 \times 10^{34}$	0.334
SAX J1748.9-2021	$6.91 \times 10^{14}$	$4.89 \times 10^{14}$	0.633	0.460	0.426	0.287	$3.22 \times 10^{34}$	$3.35 \times 10^{34}$	0.357
PSR J1614-2230	$5.46 \times 10^{14}$	$3.90 \times 10^{14}$	0.616	0.454	0.410	0.280	$2.65 \times 10^{34}$	$2.70 \times 10^{34}$	0.346
PSR J0348+0432	$5.59 \times 10^{14}$	$3.96 \times 10^{14}$	0.632	0.460	0.425	0.287	$2.61 \times 10^{34}$	$2.71 \times 10^{34}$	0.357

# More Observational Constraints

## Mass-Radius Profile

As is shown in Table 2 the surface densities of the listed pulsars,  $2.14 \times 10^{14} \lesssim \rho_R \lesssim 1.81 \times 10^{15} \text{ g/cm}^3$ , are mostly compatible with a neutron core. For four different values of the surface density of the pulsars  $\rho_R = 2.7 \times 10^{14} \text{ g/cm}^3$ ,  $4 \times 10^{14} \text{ g/cm}^3$ ,  $6 \times 10^{14} \text{ g/cm}^3$  and  $8 \times 10^{14} \text{ g/cm}^3$  we plot the corresponding compactness-radius curve. In all cases the maximum compactness values do not exceed unity. However for a compact object to be stable it should satisfy Buchdahl compactness bound  $U = \frac{2G_N M}{c^2 R} \leq 8/9$  (for isotropic sphere). We visualize Buchdahl upper bound on the compactness parameter with the corresponding maximum radii as obtained for the four surface densities.

# More Observational Constraints

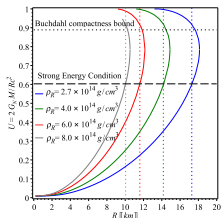
## Mass-Radius Profile

It is convenient to give the model parameters  $\{a_0, a_1, a_2\}$  in terms of the total compactness parameter  $U$ . Recalling the matching conditions (34) and (35) we write

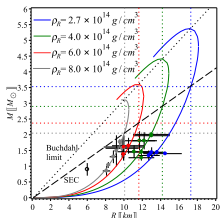
$$a_0 = \frac{3 \left\{ \left[ (U - \frac{8}{9})(1-U)^{\frac{1}{4}} + \frac{8}{9}(1-U) \right] \epsilon - \frac{1}{18}(1-U)^{\frac{1}{4}} U \right\} \sqrt{-(1-U)^2(U-2+4(1-U)^{\frac{3}{4}} - 6\sqrt{1-U} + 4(1-U)^{\frac{1}{4}})}}{\left[ -\frac{1}{2}(1-U)^{\frac{1}{4}} + \sqrt{1-U} - \frac{1}{2}(1-U)^{\frac{3}{4}} \right] (\epsilon - \frac{1}{3})(U-1)},$$
$$a_1 = -\frac{1}{2} \frac{\left( \sqrt{1-U} - (1-U)^{\frac{3}{4}} \right) a_0 + 4 \sqrt{-(1-U)^2(U-2+4(1-U)^{\frac{3}{4}} - 6\sqrt{1-U} + 4(1-U)^{\frac{1}{4}})}}{U - \sqrt{1-U} + 2(1-U)^{\frac{3}{4}} - 1},$$
$$a_2 = \sqrt{1 - (1-U)^{1/4}}. \tag{45}$$

# More Observational Constraints

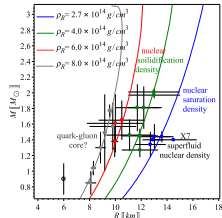
## Mass-Radius Profile



(a) Compactness-Radius



(b) Mass-Radius



(c) Neutron star core

(a) Compactness-radius profiles for four surface densities, the horizontal dot and dash lines visualize Buchdahl ( $U = 8/9$ ) and the SEC bound ( $U(\epsilon = -0.1) = 0.603$ ) on the compactness parameter. Clearly both constraints give almost the same maximum radii. (b) Mass-radius profiles for four surface densities combined with observed mass-radius values of the pulsars in Table 49. The diagonal dot and dash lines set Buchdahl and SEC physical regions. Clearly all pulsars are below the SEC exclusion limit. The horizontal dot lines give the maximum possible mass as obtained by the SEC. (c) Pulsars on the red, green and blue mass-radius profiles are suggested to have neutron cores whereas the surface densities match superfluid, saturated, solidified nuclear densities. The pulsars on the gray mass-radius profile match perfectly a surface density boundary condition  $\rho_R = 8 \times 10^{14} \text{ g/cm}^3$  which may suggest quark-gluon cores for those pulsars.

Thank you for listening.